

Lattice Boltzmann Method for Simulation of Nanoparticle Brownian Motion and Magnetic Field Effects on Free Convection in A Nanofluid-filled Open Cavity with Heat Generation/Absorption and Non Uniform Heating on the Left Solid Vertical Wall

Mohamed Ammar Abbassi¹, Bouchmel Mliki¹ and Ridha Djebali^{1,2}

Abstract: This article reports a numerical study of nanoparticle Brownian motion and magnetic field effects by natural convection in a nanofluid-filled open cavity with non uniform boundary condition. Lattice Boltzmann Method (LBM) is used to simulate nanofluid flow and heat transfer. The effective thermal conductivity and viscosity of nanofluid are calculated by KKL (Koo-Kleinstreuer-Li) correlation. In this model effect of Brownian motion on the effective thermal conductivity and effective viscosity is considered and examined. Simulations have been carried out for the pertinent parameters in the following ranges: Rayleigh number ($Ra=10^3$ - 10^6), Hartmann number ($Ha=0$ - 60), nanoparticle volume concentration ($\phi=0$ - 0.04) and heat generation or absorption coefficient ($q=-10, -5, 0, 5, 10$). The numerical results show a decrease in heat transfer with an increase in particle volume fraction. In addition, it is observed that the Brownian motion greatly influences the heat transfer rate depending on the Hartmann number, Rayleigh number and nanoparticle solid volume fraction. Additionally, in the presence of the heat generation or absorption, the Brownian motion effect on heat transfer at $Ra=10^3$ is more pronounced than other Rayleigh numbers and the least effect is observed at $Ra=10^6$.

Keywords: Brownian motion, nanofluid, heat transfer, non uniform heated cavity, lattice boltzmann method, natural convection.

Nomenclature

B	Magnetic field, T
c	Lattice speed, $m s^{-1}$
c_s	Speed of sound, $m s^{-1}$
c_i	Discrete particle speeds, $m s^{-1}$

¹ UR:Unité de Recherche Matériaux, Energie et Energies Renouvelables (MEER), Faculté des Sciences de Gafsa, B.P.19, Zarroug, Gafsa, 2112, Tunisie.

² ISLAIB-Université de Jendouba, Av. H. Bourguiba. BP 340, Béja 9000, Tunisie.

c_p	Specific heat at constant pressure, $\text{J K}^{-1} \text{kg}^{-1}$
F	External forces, N
f	Density distribution functions, kg m^{-3}
f^{eq}	Equilibrium density distribution functions, kg m^{-3}
g	Internal energy distribution functions, K
g^{eq}	Equilibrium internal energy distribution functions, K
\vec{g}	Gravity vector, m s^{-2}
Ha	Hartmann number
k	Thermal conductivity, $\text{W K}^{-1} \text{m}^{-1}$
Ma	Mach number
Nu	Local Nusselt number
P	Pressure, N m^{-2}
Pr	Prandtl number
Q_o	Heat generation or absorption, Wm^{-3}
q	Dimensionless heat generation or absorption
Ra	Rayleigh number
T	Temperature, K
$\mathbf{u}(u, v)$	Velocities, m s^{-1}
$\mathbf{x}(x, y)$	Lattice coordinates, m

Greek symbols

α	Thermal diffusivity, $\text{m}^2 \text{s}^{-1}$
Δx	Lattice spacing, m
Δt	Time increment, s
τ_a	Relaxation time for temperature, s
τ_v	Relaxation time for flow, s
ν	Kinematic viscosity, $\text{m}^2 \text{s}^{-1}$
ρ	Fluid density, kg m^{-3}
ψ	Non-dimensional stream function
ϕ	Solid volume fraction, Wm^{-3}
μ	Dynamic viscosity, $\text{kg m}^{-1} \text{s}^{-1}$
γ	Inclination angle of magnetic field
θ	Non-dimensional temperature

Subscript

f	Fluid
nf	Nanofluid
p	particle

1 Introduction

The study of heat transfer enhancement in open cavities has been widely investigated due to its relevance in some thermal engineering applications such as solar collectors having insulated strips [Sezai, Mohamad (1999)], domestic refrigerators and ovens [Skok, Ramadhyani and Schoenhals (1991)], electronic cooling devices [Lage, Lim and Bejan (1992)] and other industrial systems in various sectors. It must also be noted that the heat transfer enhancement by means of nanofluids is still an important subject. Much attention has been paid in the past decade to this new type of nanofluid because of its behaviour associated with heat transfer. Various investigations on Magnetohydrodynamic (MHD) natural convection were implemented by researchers. [Mliki, Abbassi and Omri (2015)] used the lattice Boltzmann method to simulate the nanofluid free double dispersion natural convection inside in a C-shaped enclosure. The nanofluid thermal conductivity is chosen in such a way that it takes into account the Brownian motion and temperature field effects in addition to the nanoparticle volume concentration. The effect of magnetic field on heat transfer in the C-shaped enclosure is studied.

Investigations on natural convection in open cavities in the presence of a magnetic field were done by researchers with different numerical methods. Especially, in order to understand buoyancy-driven heat transfer of nanofluids in a cavity several investigations have been numerically and experimentally conducted. The numerical investigation of natural convection in an open ended rectangular cavity has been carried out by using lattice Boltzmann method (LBM) at various physical flow governing parameters such as Rayleigh number ($10^4 \leq Ra \leq 10^6$) and aspect ratio ($0.5 \leq AR \leq 10$) by [Mohamad, El-Ganaoui and Bennacer (2009)]. They reported inverse dependence of the rate of heat transfer on the aspect ratio based on the use of D_2Q_4 and D_2Q_9 lattice models for the thermal and flow fields, respectively. [Mahmoudi, Mejri, Abbassi and Omri (2015)] investigated MHD natural convection flow and heat transfer in open cavity filled with nanofluids, utilizing non uniform boundary condition and in the presence of uniform heat generation/absorption by using lattice Boltzmann method. The presented results indicated the decrease in heat transfer rate with Hartmann number and linear variation with Rayleigh number. In the same period, [Mejri and Mahmoudi (2015)] have performed a numerical study using the Lattice Boltzmann method in a nanofluid-filled open enclosure with a sinusoidal boundary condition. The study was carried out by using physical flow governing parameters, such as, Rayleigh number ($Ra=10^3-10^6$), Hartmann number ($Ha=0-60$), the solid volume fraction of the nanoparticles between $\phi=0$ and 6% and phase deviation ($\gamma=0, \pi/4, \pi/2, 3\pi/4$ and π). The presented results showed that for $Ra=10^3$ to 10^5 and $Ha=30$, for all phase deviations the addition of nanoparticles increases heat transfer rate. In addition, the authors have concluded that, the highest heat transfer rate is obtained

for low Rayleigh number ($Ra \leq 10^4$) and phase deviation ($\gamma = \pi/2$). [Kefayati (2013)] investigated numerically natural convection in an open cavity in the presence of magnetic field at various physical flow governing parameters such as ($Ra = 10^3 - 10^6$) the solid volume fraction of the nanoparticles between $\phi = 0$ and 6% and Hartmann number ($Ha = 0 - 90$) by using Lattice Boltzmann method. The results presented show that the rate of heat transfer is an increasing function of Hartmann number. [Hussein, Ashorynejad, Shikholeslami and Sivasankaran (2014)] examined numerically natural convection in an open enclosure filled with nanofluids in the presence of magnetic field. In this study, the effective thermal conductivity and viscosity of nanofluid were calculated by the Maxwell-Garnett (MG) and Brinkman models, respectively. The influence of pertinent parameters such as Rayleigh number, nanoparticle volume fraction, Hartmann number and the inclination of magnetic field on the flow and heat transfer characteristics have been examined. They demonstrated that the absolute values of stream function rise by increasing Rayleigh numbers while these values decline significantly by increasing Hartmann numbers. Also, it was found that the magnetic field orientation angle increases, the flow circulation intensity and the convection effect begins to decrease. Subsequently [Gangawane, Bharti and Kumar (2016)] simulated the TLBM MHD natural convection in an open ended rectangular cavity at various physical flow governing parameters such as Rayleigh number ($Ra = 10^3 - 10^6$), heating location (bottom, middle, and top) on west wall and dimensionless heating length ($L = 0.25 - 0.75$) on the flow and temperature fields. They found that the maximum heat transfer is observed in the case of middle heating. Also, they reported linear dependence of the average Nusselt number (Nu) on the Rayleigh number, irrespective of the heating locations and heater size. In another study, [Gangawane, Bharti and Kumar (2015)] numerically investigated the natural convection in an open ended rectangular cavity at various physical flow governing parameters such as Rayleigh number ($Ra = 10^3 - 10^6$), heating location (bottom, middle, and top) and Prandtl number ($Pr = 0.71$) by using passive scalar thermal lattice Boltzmann method (PS-TLBM) with $D2Q9$ (two-dimensional and nine-velocity link) lattice model. They showed that the middle heating location gives higher heat transfer rate than that for the top and bottom heating cases. Also, it was found that the average Nusselt number increases with Rayleigh number. In addition, the influence of a Brownian motion of nanoparticles in a nanofluid has been explored well over the last few decades. [Ghasemi and Aminossadati (2010)] reported the Brownian motion effects in a triangular enclosure with natural convection. The effect of partial heating locations, Rayleigh number, solid volume fraction, enclosure aspect ratio and Brownian motion have been presented and discussed. They observed that the heat transfer of the nanofluid increases when considering the Brownian motion. Moreover, when Brownian motion is considered, an optimum solid volume fraction can be found, which results in the maximum heat transfer rate. This is in contradiction to the results of the analysis in which Brownian motion is neglected when the heat transfer rate continuously increases with the solid volume fraction. [Haddad, Abu Nada and Oztop (2012)] numerically investigated the convection fluid flow and heat transfer and fluid flow of CuO-water nanofluid in a cavity heated from the bottom. In this study, the effect of Brownian motion on the effective thermal conductivity and effective viscosity is considered. Results indicated that the enhancement in heat transfer is

observed at any Rayleigh numbers and nanoparticle volume fraction by considering the role of Brownian motion.

The main aim of the present work is to discuss the effect of Brownian motion on heat transfer in a nanofluid-filled open cavity with non uniform boundary condition. The results will be presented in this work via streamlines, isotherms, average Nusselt number at different nanoparticle volume fractions, Hartman and Rayleigh numbers.

2 Mathematical formulation

2.1 Problem statement and mathematical modeling

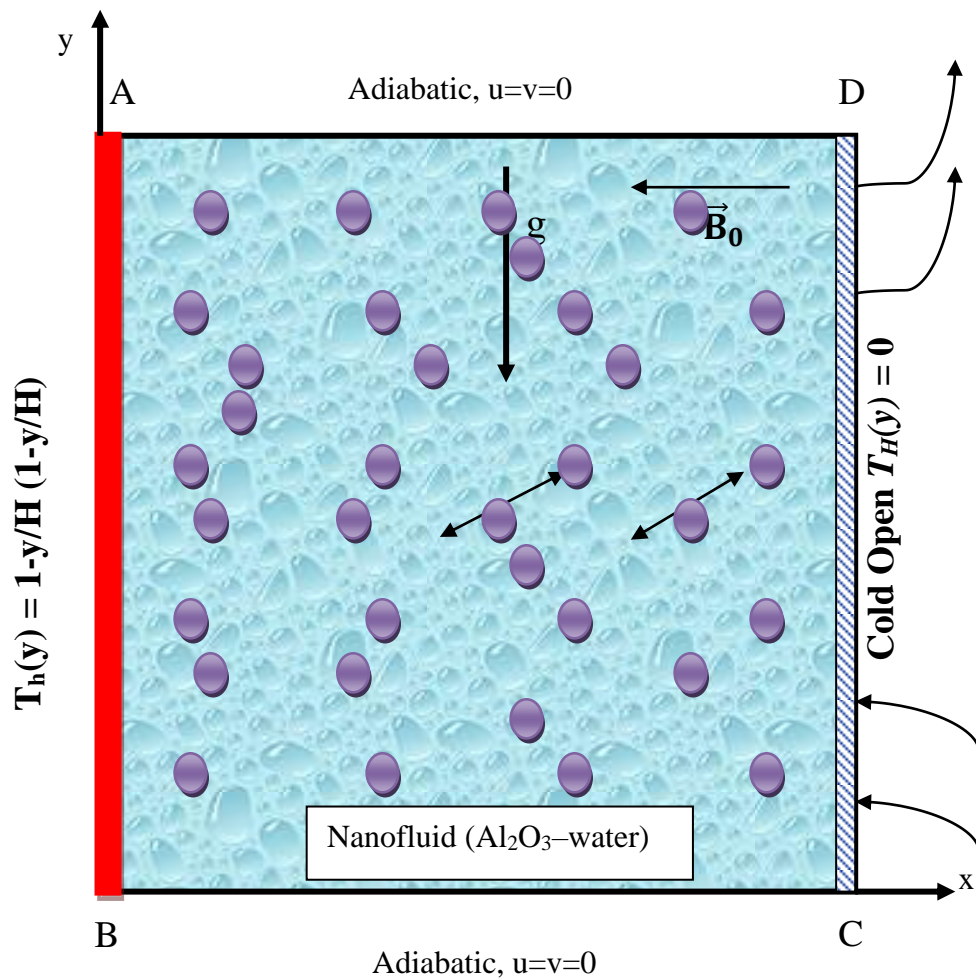


Figure 1: Geometry of the present study with boundary conditions

The considered physical geometry of the present problem with related parameters and coordinates are shown in Figure 1. It consists of a two-dimensional open cavity with the

height of H . The left wall is maintained to a non uniform boundary condition $T_h(y) = 1 - y/H (1 - y/H)$. An external cold nanofluid enters into the enclosure from the east opening boundaries while the Al_2O_3 -water nanofluid is correlated with the opening boundary at the constant temperature of T_c . The bottom and top walls of cavity are thermally insulated. A uniform magnetic field of magnitude B is applied in the horizontal direction. The cavity walls are electrically insulated. The thermo-physical properties of the base fluid and the nanoparticles are given in Table 1. The magnetizing force due to the weak magnetic dipoles moment is neglected compared to the Lorentz force. Furthermore, it is assumed that the viscous dissipation and Joule heating are neglected.

Table 1: Thermo physical properties of fluid and nanoparticles [Sheikholeslami (2013)]

Physical Properties	Fluid (Water)	phase	Al_2O_3 (nanoparticles)
C_p (J/kgK)	4179		385
ρ (kg/m ³)	997.1		8933
k (W/mK)	0.631		400
$\beta \times 10^{-5}$ (1/K)	21		1.6
σ (Ωm) ⁻¹	0.05		1×10^{-10}

The equations governing the Magnetohydrodynamic (MHD) natural convection flow and heat transfer, namely, continuity, Navier–Stokes, and the thermal energy equations in nondimensional form, are given as follow:

$$\frac{\partial u}{\partial x} + \frac{\partial v}{\partial y} = 0 \quad (1)$$

$$\rho_{nf} \left(u \frac{\partial u}{\partial x} + v \frac{\partial u}{\partial y} \right) = -\frac{\partial p}{\partial x} + \mu_{nf} \left(\frac{\partial^2 u}{\partial x^2} + \frac{\partial^2 u}{\partial y^2} \right) \quad (2)$$

$$\rho_{nf} \left(u \frac{\partial v}{\partial x} + v \frac{\partial v}{\partial y} \right) = -\frac{\partial p}{\partial y} + \mu_{nf} \left(\frac{\partial^2 v}{\partial x^2} + \frac{\partial^2 v}{\partial y^2} \right) + (\rho\beta_T)_{nf} g(T - T_c) - B^2 \cdot \sigma_{nf} v \quad (3)$$

$$u \frac{\partial T}{\partial x} + v \frac{\partial T}{\partial y} = \alpha_{nf} \left(\frac{\partial^2 T}{\partial x^2} + \frac{\partial^2 T}{\partial y^2} \right) + \frac{Q}{(\rho C_p)_{nf}} (T - T_c) \quad (4)$$

where σ_{nf} is electrical conductivity of nanofluid, B is the magnitude of the magnetic field and Q is the heat generation or absorption coefficient.

The effective density (ρ_{nf}), the thermal expansion coefficient (β_{nf}), heat capacitance $(\rho C_p)_{nf}$ and thermal diffusivity of the nanofluid are respectively defined by [Xuan and Roetzel (2000)]:

$$\rho_{nf} = (1 - \phi)\rho_f + \phi\rho_p \quad (5)$$

$$(\rho C_p)_{nf} = (1-\phi)(\rho C_p)_f + \phi(\rho C_p)_p \quad (6)$$

$$(\rho\beta)_{nf} = (1-\phi)(\rho\beta)_f + \phi(\rho\beta)_p \quad (7)$$

$$\alpha_{nf} = \frac{k_{nf}}{(\rho C_p)_{nf}} \quad (8)$$

For thermal conductivity, we used the model developed by [Koo and Kleinstreuer (2004)] that considers the nanoparticle Brownian motion. This model takes into account the effects of particle volume fraction, particle size and nanofluid temperature.

$$k_{eff} = k_{static} + k_{Brownian} \quad (9)$$

Where k_{static} is the static thermal conductivity based on Maxwell classical correlation and $k_{Brownian}$ is the component considered the enhanced thermal conductivity by micro-scale convective heat transfer of a particle's Brownian motion.

$$k_{static} = k_f \frac{k_p + 2k_f - 2\phi(k_f - k_p)}{k_p + 2k_f + \phi(k_f - k_p)} \quad (10)$$

$$k_{Brownian} = 5 \times 10^4 \beta \phi \rho_f C_p \sqrt{\frac{k_b T}{\rho_p d_p}} f(T, \phi) \quad (11)$$

where (β and f), two empirical functions combined the interaction between nanoparticles.

$$\beta = 0.0137(100\phi)^{-0.8229} \quad \text{for } \phi < 1\% \quad (12)$$

$$\beta = 0.0011(100\phi)^{-0.7272} \quad \text{for } \phi \geq 1\% \quad (13)$$

$$f(T, \phi) = (-6.04\phi + 0.4705)T + (1722.3\phi - 134.63) \quad \text{for } 1\% \leq \phi \leq 4\% \quad (14)$$

This equation is valid for temperatures in the range of $300 \text{ K} \leq T \leq 325 \text{ K}$

The effective viscosity of the nanofluid containing a dilute suspension of small rigid spherical particles is given by as [Koo and Kleinstreuer (2005)]:

$$\mu_{eff} = \mu_{static} + \mu_{Brownian} \quad (15)$$

where μ_{static} is the viscosity of the nanofluid, as given originally by [Brinkman (1952)] and $\mu_{Brownian}$ is the component considered the effective viscosity due to Brownian motion of a particle's proposed by [Koo and Kleinstreuer (2005)].

$$\mu_{static} = \frac{\mu_f}{(1-\phi)^{2.5}} \quad (16)$$

$$\mu_{Brownian} = 5 \times 10^4 \beta \phi \rho_f \sqrt{\frac{k_b T}{\rho_p d_p}} f(T, \phi) \quad (17)$$

Also, effective electrical conductivity of nanofluid was presented by [Sheikholeslami, Gorji-Bandpy, Ellahi and Zeeshan (2014)] as below:

$$\frac{\sigma_{nf}}{\sigma_f} = 1 + \frac{3\left(\frac{\sigma_s}{\sigma_f} - 1\right)\phi}{\left(\frac{\sigma_s}{\sigma_f} + 2\right) - \left(\frac{\sigma_s}{\sigma_f} - 1\right)\phi} \quad (18)$$

The governing equations (1-4) are made dimensionless using the following dimensionless variables:

$$X = \frac{x}{L}, \quad Y = \frac{y}{L}, \quad U = \frac{uL}{\alpha_{nf}}, \quad V = \frac{vL}{\alpha_{nf}}, \quad \theta = \frac{T - T_c}{T_h - T_c}, \quad P = \frac{pL^2}{\rho_{nf}\alpha_{nf}^2} \quad (19)$$

$$Pr = \frac{\nu_{nf}}{\alpha_{nf}}, \quad Ra = \frac{g\beta(T - T_c)L^3}{\nu_{nf}\alpha_{nf}}, \quad q = \frac{Q_0L^2}{(\rho c_p)_{nf}\alpha_{nf}}, \quad Ha = HB\sqrt{\frac{\sigma_{nf}}{\mu_{nf}}}$$

Based on the dimensionless variables above, equations (1-4) can be written as follows:

$$\frac{\partial U}{\partial X} + \frac{\partial V}{\partial Y} = 0 \quad (20)$$

$$U \frac{\partial U}{\partial X} + V \frac{\partial U}{\partial Y} = -\frac{\partial P}{\partial X} + Pr^* \left(\frac{\partial^2 U}{\partial X^2} + \frac{\partial^2 U}{\partial Y^2} \right) \quad (21)$$

$$U \frac{\partial V}{\partial X} + V \frac{\partial V}{\partial Y} = -\frac{\partial P}{\partial Y} + Pr^* \left(\frac{\partial^2 V}{\partial X^2} + \frac{\partial^2 V}{\partial Y^2} \right) + Ra^* Pr^* \theta - Ha^2 Pr^* V \quad (22)$$

$$U \frac{\partial \theta}{\partial X} + V \frac{\partial \theta}{\partial Y} = \left(\frac{\partial^2 \theta}{\partial X^2} + \frac{\partial^2 \theta}{\partial Y^2} \right) + q\theta \quad (23)$$

where

$$Pr^* = \frac{\mu_{nf} C_{p_{nf}} k_f}{\mu_f C_{p_f} k_{nf}} Pr, \quad Ra^* = \frac{(\rho\beta)_{nf} k_f (\rho C)_{p_{nf}} \mu_f}{(\rho\beta)_f k_{nf} (\rho C)_{p_f} \mu_{nf}} Ra \quad (24)$$

3 Simulation of MHD & nanofluid with lattice boltzmann method

3.1 Brief Introduction to LBM

The Lattice Boltzmann Method (LBM) was based on Ludwig Boltzmann's kinetic theory of gases. The fundamental idea is that gases/fluids can be a large number of small particles moving with random motions. The exchange of momentum and energy is achieved through particle streaming and collision. For the incompressible non isothermal problems, (LBM) utilizes two distribution functions f and g , for the flow and temperature fields respectively.

For the flow field:

$$f_i(\mathbf{x} + \mathbf{c}_i \Delta t, t + \Delta t) = f_i(\mathbf{x}, t) - \frac{1}{\tau_\nu} \left(f_i(\mathbf{x}, t) - f_i^{\text{eq}}(\mathbf{x}, t) \right) + \Delta t \mathbf{c}_i F_i \quad (25)$$

For the temperature field:

$$g_i(\mathbf{x} + \mathbf{c}_i \Delta t, t + \Delta t) = g_i(\mathbf{x}, t) - \frac{1}{\tau_\alpha} (g_i(\mathbf{x}, t) - g_i^{\text{eq}}(\mathbf{x}, t)) \quad (26)$$

Where the discrete particle velocity vectors is defined by \mathbf{c}_i . Δt denotes lattice time step which is set to unity. τ_v and τ_α are the relaxation time for the flow and temperature fields, respectively. f_i^{eq} and g_i^{eq} are the local equilibrium distribution functions that have an appropriately prescribed functional dependence on the local hydrodynamic properties which are calculated with Eqs. (5)-(18) and for flow and temperature fields respectively.

$$f_i^{\text{eq}} = \omega_i \rho \left[1 + \frac{3(\mathbf{c}_i \cdot \mathbf{u})}{c^2} + \frac{9(\mathbf{c}_i \cdot \mathbf{u})^2}{2c^4} - \frac{3\mathbf{u}^2}{2c^2} \right] \quad (27)$$

$$g_i^{\text{eq}} = \omega_i' T \left[1 + 3 \frac{\mathbf{c}_i \cdot \mathbf{u}}{c^2} \right] \quad (28)$$

\mathbf{u} and ρ are the macroscopic velocity and density, respectively. c is the lattice speed which is equal to $\Delta x / \Delta t$ where Δx is the lattice space similar to the lattice time step Δt which is equal to unity, ω_i is the weighting factor for flow and ω_i' is the weighting factor for temperature. The D2Q9 and D2Q4 lattice models are applied to present study. According to these models, the weighting factors and the discrete particle velocity vectors can be calculated with Eqs (29-31):

For D2Q9

$$\omega_0 = \frac{4}{9}, \omega_i = \frac{1}{9} \text{ for } i=1,2,3,4 \text{ and } \omega_i = \frac{1}{36} \text{ for } i=5,6,7,8 \quad (29)$$

$$\mathbf{c}_i = \begin{cases} 0 & i=0 \\ (\cos[(i-1)\pi/2], \sin[(i-1)\pi/2])c & i=1,2,3,4 \\ \sqrt{2}(\cos[(i-5)\pi/2 + \pi/4], \sin[(i-5)\pi/2 + \pi/4])c & i=5,6,7,8 \end{cases} \quad (30)$$

For D2Q4

The temperature weighting factor for each direction is equal to $\omega_i' = 1/4$.

$$\mathbf{c}_i = (\cos[(i-1)\pi/2], \sin[(i-1)\pi/2])c \quad i=1,2,3,4 \quad (31)$$

The kinematic viscosity ν and thermal diffusivity α are respectively related to the relaxation time by Eq. (32):

$$\nu = \left[\tau_v - \frac{1}{2} \right] c_s^2 \Delta t, \quad \alpha = \left[\tau_\alpha - \frac{1}{2} \right] c_s^2 \Delta t \quad (32)$$

Where c_s is the lattice speed of sound which is equal to $c_s = c/\sqrt{3}$. In the simulation of natural convection, the external force term F_i is given by Eq. (33):

$$F_i = \frac{\omega_i}{c_s^2} F \cdot \mathbf{c}_i \quad (33)$$

With F is the total external body force.

The macroscopic quantities ρ , u and T can be calculated respectively by Eqs. (34)-(36).

$$\rho = \sum_i f_i \quad (34)$$

$$\rho u = \sum_i f_i \mathbf{c}_i \quad (35)$$

$$T = \sum_i g_i \quad (36)$$

3.2 Implementation of boundary conditions

One of the important and crucial issues in LBM simulation of flow and temperature is accurate modeling of the boundary conditions. Therefore, we need to determine appropriate equations for calculating those distribution functions f and g , for the flow and temperature at the boundaries for a given boundary condition.

3.2.1 Flow

Bounce-back boundary conditions were applied on all solid boundaries, which mean that incoming boundary populations are equal to out-going populations after the collision. The unknown density distribution functions at the left, south and north walls of the cavity can be determined by the following conditions respectively (Figure 2. a):

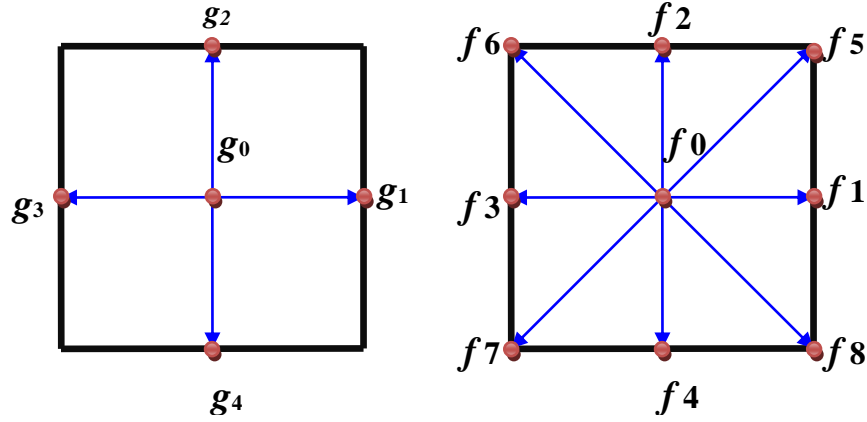
$$f(1,0) = f(3,0); f(5,0) = f(7,0); f(8,0) = f(6,0) \quad (37)$$

$$f(0,5) = f(0,7); f(0,2) = f(0,4); f(0,6) = f(0,8) \quad (38)$$

$$f(m,7) = f(m,5); f(m,4) = f(m,2); f(m,8) = f(m,6) \quad (39)$$

where m is a boundary node on the east wall ($x = L$).

The flow field boundary condition at the open right wall of cavity is implemented as below:



(a) D2Q4 (For Temperature) (b) D2Q9 (For Flow)

Figure 2: Domain boundaries and direction of streaming velocities.

$$f(3,n)=f(3,n-1); f(6,n)=f(6,n-1); f(7,n)=f(7,n-1) \quad (40)$$

where n is a boundary node on the open end ($x = L$) side.

3.2.2 Temperature

Bounce back boundary condition (adiabatic) is used on the top and bottom walls of the cavity. The following conditions at the adiabatic walls (top and bottom) can be determined respectively by (Figure 2. b):

$$g(1,0)=g(1,1); g(2,0)=g(2,1); g(3,0)=g(3,1); g(4,0)=g(4,1); g(0,0)=g(0,1) \quad (41)$$

$$g(1,0)=g(1,1); g(2,0)=g(2,1); g(3,0)=g(3,1); g(4,0)=g(4,1); g(0,0)=g(0,1) \quad (42)$$

Since we are using D_2Q_4 model, the unknowns for the left and the right open wall are respectively $g(1,0)$ and $g(3,0)$ which are evaluated as, (Figure 2. b):

- For the left boundary, the following conditions are imposed:

$$g(1,0)=T_h(y) (w(1)+w(3))- g(3,0) \quad (43)$$

- On the right wall the temperature boundary condition is calculated depending on fluid motion. If the fluid enters the cavity it is supposed to have a cold temperature, whereas if it exits the cavity we suppose that the right wall is adiabatic.

$$\text{Right wall} \begin{cases} \text{if } u > 0 \text{ then } \left. \frac{\partial T}{\partial x} \right|_{x=H} = 0 \\ \text{if } u < 0 \text{ then } T(H, y) = T_c \end{cases}$$

$$g(3, n) = -g(1, n) \text{ for } u < 0; \quad g(3, n) = g(3, n-1) \text{ for } u > 0 \quad (44)$$

3.3 Solution method

To ensure that the code is applicable in a near incompressible regime, the characteristic velocity must be small compared to the fluid speed of sound. Hence, in simulation, Mach number should be less than $Ma = 0.3$. Therefore, for all the considered cases in the present study, Mach number is fixed as 0.1. By fixing Rayleigh number, Prandtl number and Mach number, the viscosity and thermal diffusivity are calculated from the definition of these non dimensional parameters.

$$v_f = NMac_s \sqrt{\frac{Pr}{Ra}} \quad (45)$$

With N is the number of lattices in y -direction.

Nusselt number Nu is one of the most important dimensionless parameters in describing the convective heat transport. The local Nusselt number at the right and left walls is expressed as:

$$Nu_l = \frac{hH}{k_f} \quad (46)$$

The thermal conductivity of the nanofluid is expressed as:

$$k_{nf} = -\frac{q_w}{\partial T / \partial x} \quad (47)$$

where the heat transfer coefficient is given by:

$$h = \frac{q_w}{T_h - T_c} \quad (48)$$

Substituting Eqs. (47) and (48) into Eq. (46), and using the dimensionless quantities, we get the local Nusselt number along the left wall as:

$$Nu_l = -\frac{k_{nf}}{k_f} \left(\frac{\partial \theta}{\partial X} \right) \Big|_{X=0} \quad (49)$$

Accordingly, the average Nusselt number can be obtained as:

$$\overline{Nu}_l = -\frac{1}{H} \int_0^H \frac{k_{nf}}{k_f} \left(\frac{\partial \theta}{\partial X} \right) \Big|_{X=0} \quad (50)$$

The stream function and vorticity are defined as:

$$\frac{\partial^2 \psi}{\partial x^2} + \frac{\partial^2 \psi}{\partial y^2} = -\left(\frac{\partial v}{\partial x} - \frac{\partial u}{\partial y} \right) = -\omega \quad (51)$$

where ω and ψ are vorticity and stream function, respectively.

4 Code validation and grid independence

Figure 3 demonstrates the effect of grid resolution and the lattice sizes by calculating the average Nusselt number on the left wall for the case of $Ra=10^4$ and 10^5 . The grid independence study is carried out by using the five uniform grid lattice sizes (40x40, 60x60, 80x80, 100x100, 120x120 and 140x140). It is found that a grid size of 100×100 ensures the grid independent solution for this case. In order to verify the accuracy of the present numerical study, the present numerical model was validated at the three topics of this previous problem. For the first part, Figure4 shows the comparison of the temperature on axial midline computed for three values of the Hartmann number ($Ha=0, 30, 60$), Rayleigh number ($Ra=10^5$) and for a solid volume fraction $\phi = 0.03$, between the present calculations and the results of [Ghassemi and Aminossadati (2010)] for MHD natural convection in an enclosure filled with Cu–water nanofluid. At the second part, the comparison of streamlines and isotherms obtained showed a very good agreement with those of [Mohamad, El-Ganaoui and Bennacer (2009)] for $Ra = 10^4$ (Figure5). Furthermore, Table 2 shows the comparison of average Nusselt number at the hot wall of the present study with the prediction of LBM [Mahmoudi, Mejri, Abbassi and Omri (2015)] and Finite Volume Method (FVM) [Mohamad, El-Ganaoui and Bennacer (2009)].

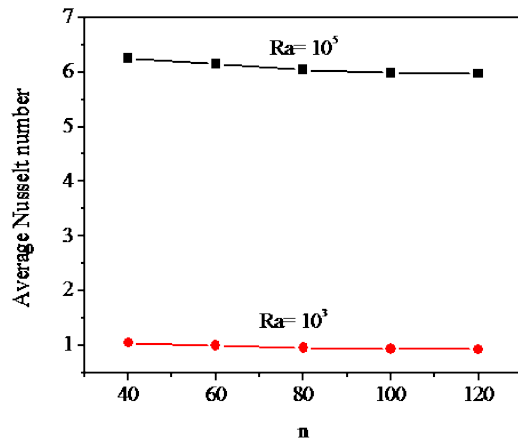


Figure 3. Average Nusselt number on the left wall for different uniform grids for $q=0, Ha=0$ and $\phi=0$.

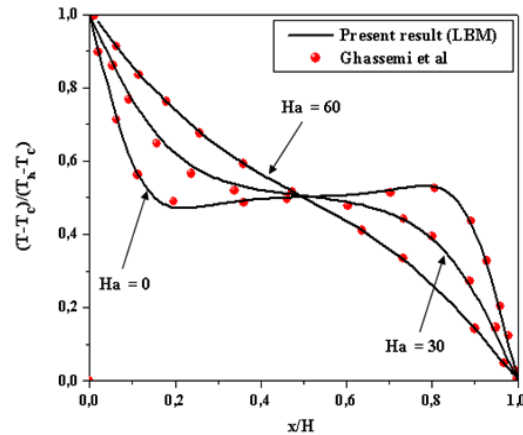


Figure 4. Comparison of the temperature on axial midline between the present results and numerical results by Ghassemi et al. (2010) ($\phi=0.03, Ra=10^5$).

These comparisons show that the present study has a good agreement with previous studies.

Table 2: Comparison of average Nusselt number at hot wall

Ra	Present	[Mejri and Mahmoudi, 2015]	[Mohammad, 2009]
$Ra = 10^4$	3.263	3.250	3.264
$Ra = 10^5$	7.217	7.237	7.261
$Ra = 10^6$	14.250	14.222	14.076

5 Results and discussion

Lattice Boltzmann Method (LBM) is applied to perform the analysis of laminar free convection heat transfer and fluid flow in an open square cavity containing water-based nanofluid. Effects of the parameters Rayleigh number (Ra), Hartmann number (Ha), volume fraction of the nanoparticles (ϕ) and the heat generation or absorption coefficients (q) on heat transfer and fluid flow inside the cavity has been studied. Comparison of two cases as absence of Brownian effect and presence of Brownian effect will be discussed. The isotherms and streamlines with all Ra , Ha and q in this work have been affected by the Brownian motion of nanoparticles. Figs. 6–7 illustrate the effect of Rayleigh number and Hartmann number, on the isotherms and streamlines of nanofluid ($\phi=0.04$) for $q=0$. It is obvious that the isotherms near to the hot wall as Rayleigh number augments at different Hartmann numbers and heat transfer by convection dominates. This is because the buoyancy force effect is important, so the convection heat transfer contribution is important too and the conduction heat transfer is neglected.

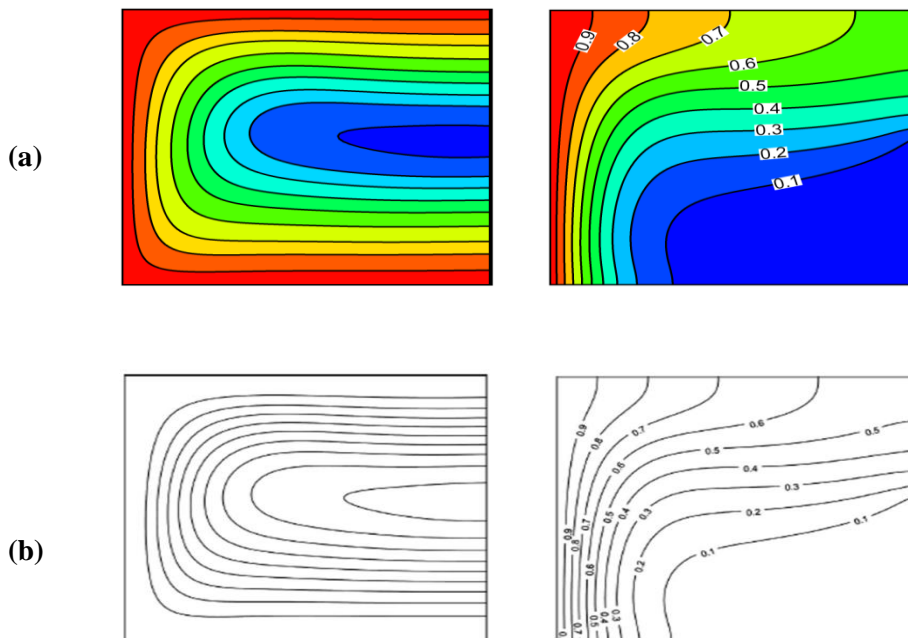
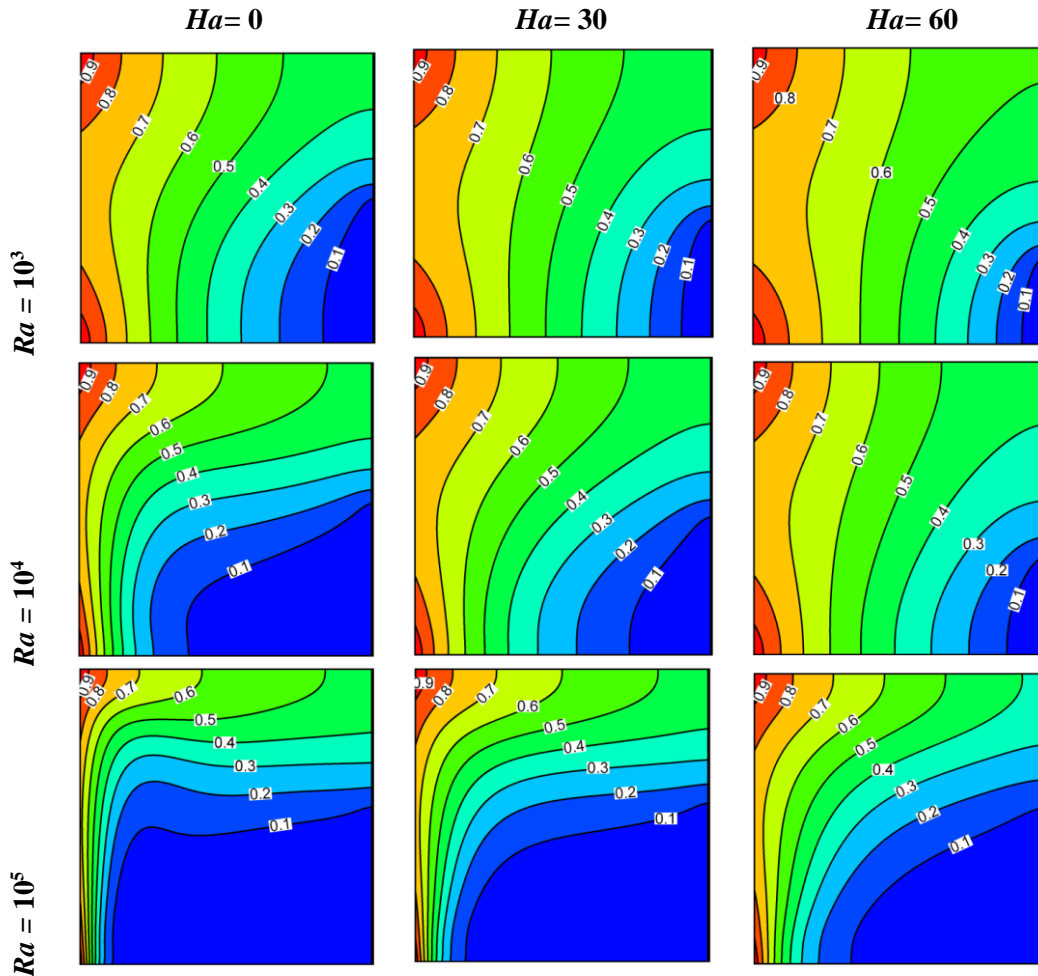


Figure 5: Comparison of the streamlines and isotherms between (a) numerical results by [Mohammad, El-Ganaoui and Bennacer (2009)] and (b) the present results.

Also, the increase in Rayleigh number causes to occur an almost isothermal process at down half of open enclosure. On the contrary, it is noticeable that the gradient of temperature on the hot wall decreases as the Hartmann number increases. This occurs due to the magnetic damping effect that suppresses the overall heat transfer in the open square cavity. For the streamlines, it is shown that the maximum value of the stream function decreases with the rise of Hartmann number for all Rayleigh numbers. But the effect of Hartmann number is not identical for different Rayleigh numbers. For instance, for $Ha=0$ to 60 the values of the maximum stream function decrease by 96%, 91%, 73% and 54% for Rayleigh numbers of $Ra=10^3$, 10^4 , 10^5 and 10^6 respectively. So, the trend exhibits that The effect of the magnetic field on the fluid flow drops with the rise of Rayleigh number.

Existence of the nanoparticles in the water changes the properties of the base fluid and hence affects the heat transfer and fluid flow characteristics. The presence of high thermal conductive nanoparticles enhances the thermal conductivity of the nanofluids and causes a favorable enhancement of the heat transfer.



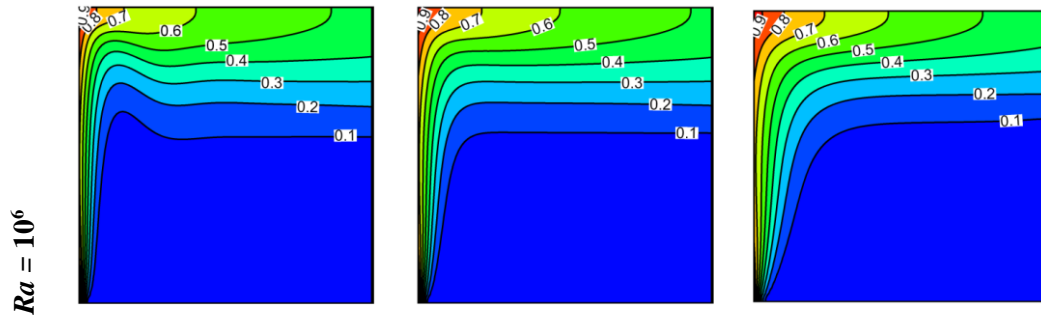
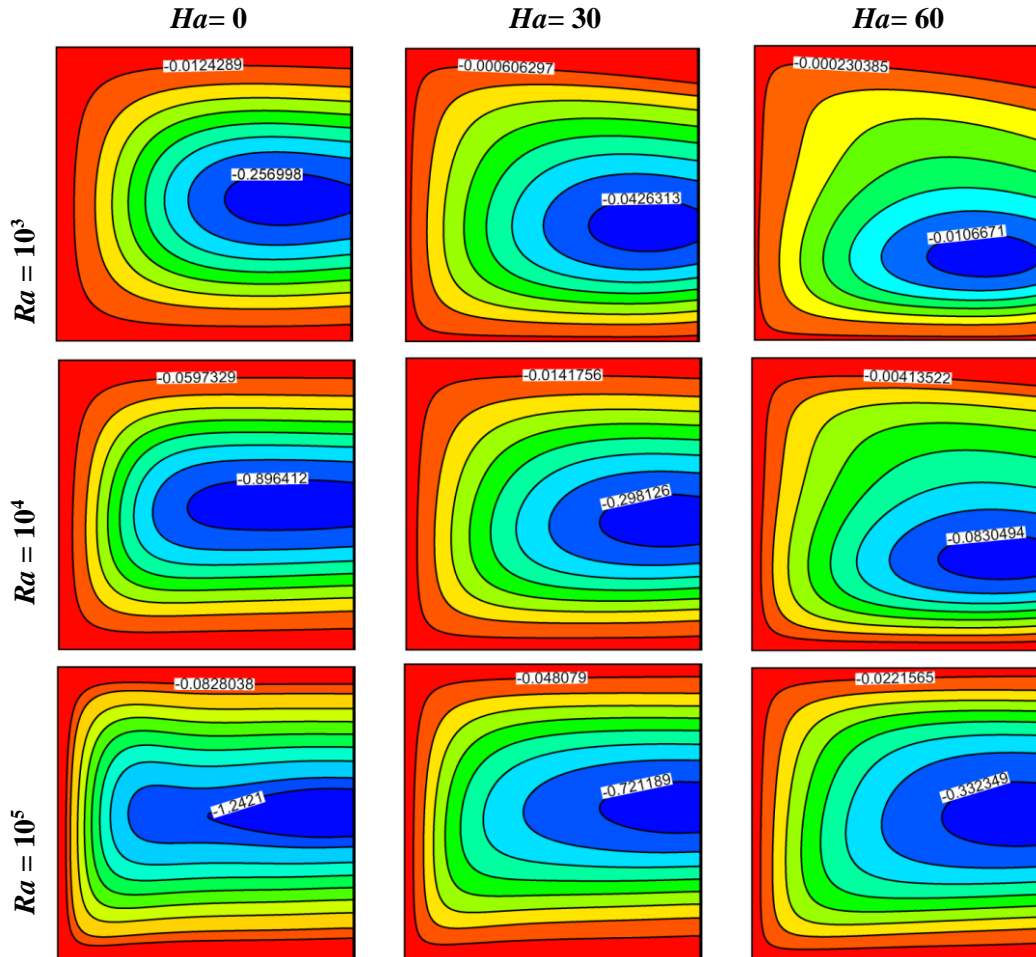


Figure 6: Isotherms for different Ra and Ha at $q = 0$ and $\phi = 0.04$ (water- Al_2O_3 nanofluid).

On the other hand, the increase of nanofluid viscosity decreases convection heat transfer. So, this last effect of nanoparticles is unfavorable from the point of view of heat transfer.



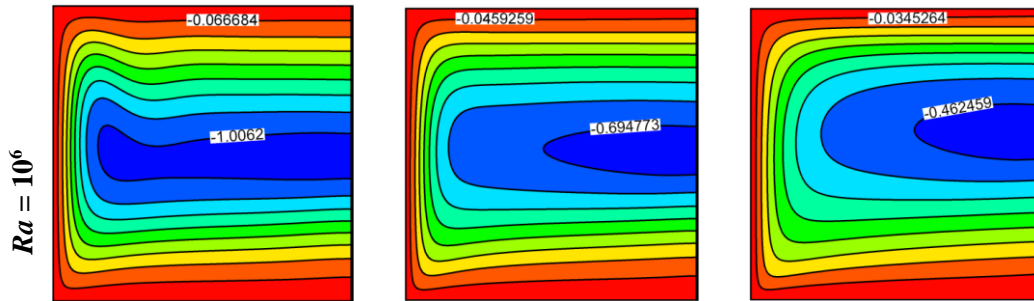


Figure 7: Streamlines for different Ra and Ha at $q = 0$ and $\phi = 0.04$ (water- Al_2O_3 nanofluid).

As can be seen in Figure 8 the Brownian motion effect on the variation of average Nusselt number for, $Ha=0$, $q=0$, $\phi=0.04$ and different Rayleigh numbers ($Ra=10^3$, 10^5) will be presented. A comparison between the two studies of with and without Brownian motion shows that the heat transfer is generally higher when Brownian motion is considered. When Brownian motion is neglected ($k_{eff} = k_{static}$, $\mu_{eff} = \mu_{static}$), the average Nusselt number continuously increases as ϕ increases for all Rayleigh numbers. However, when Brownian motion is considered ($k_{eff} = k_{static} + k_{Brownian}$, $\mu_{eff} = \mu_{static} + \mu_{Brownian}$), an optimum value for ϕ can be found which results in the maximum Nu_{max} . This result agrees well with published results by [Ghasemi and Aminossadati (2010)] and [Haddad, Abu-Nada, Oztop and Mataoui (2012)]. At $Ra=10^3$, the Brownian motion effect acts as an effective parameter to augment heat transfer when $\phi < 0.03$. On contrast, when the solid volume fraction increases from $\phi= 0.03$ to 0.04 , the average Nusselt number decreases. Therefore, the Brownian motion effect on the enhancement appears at low volume fraction of the nanoparticles. So, the favorable enhancement of the nanofluid has a dominant effect on the thermal conductivity, it leads to enhancement of the Nusselt numbers, but the unfavorable increase of the nanofluid viscosity affects on some amount of this enhancement. But, on the contrary at high values of the solid volume fraction, the Brownian motion of the nanoparticles has an adverse effect on heat transfer. This is due to make the nanofluid to be more viscous, which will reduce convection currents and accordingly will diminish the temperature gradient and the Nusselt number at the heated surface. At $Ra=10^5$, the average Nusselt number changes with the similar trend of $Ra = 10^3$, just the optimum value for ϕ equal to 0.02 .

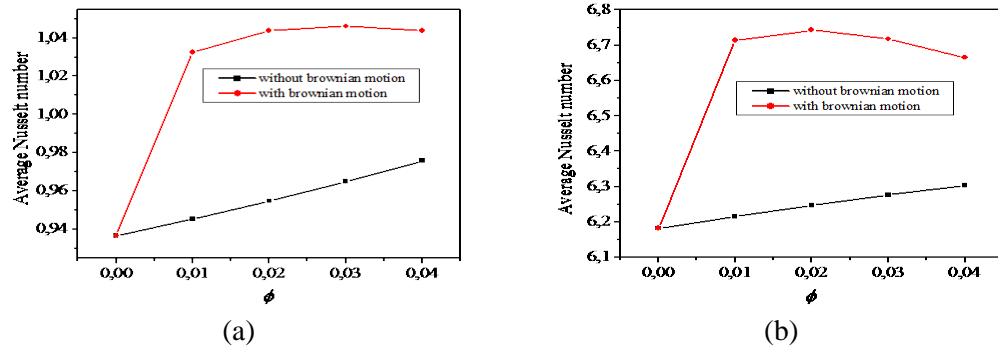


Figure 8: Average Nusselt number on the left wall for different Ra and ϕ , (a) $Ra=10^3$, (b) $Ra=10^5$ at $q=0$.

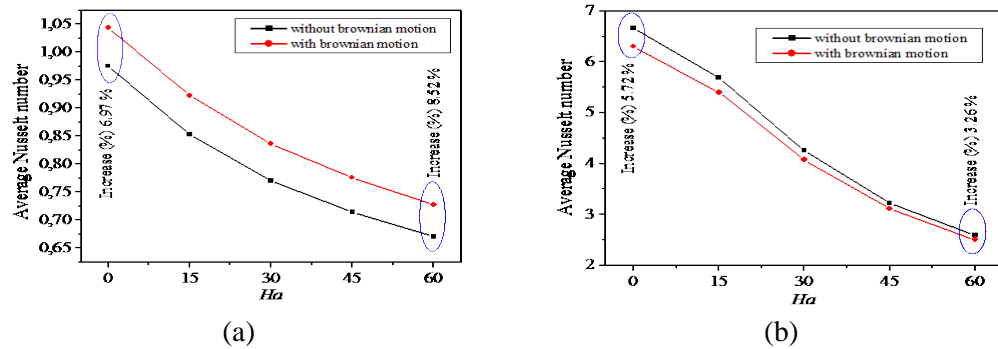


Figure 9: Average Nusselt number on the left wall for different Ra and Ha , (a) $Ra=10^3$, (b) $Ra=10^5$ at $q=0$.

Figure 9 presents the average Nusselt number for the nanofluid at various Rayleigh numbers ($Ra=10^3, 10^5$) and Hartman number ($Ha = 0, 15, 30, 45, 60$). The influence of Brownian motion on the Nu_m is more significant in the conduction regime which is illustrated for $Ra = 10^3$. More specifically, at $Ra = 10^3$, when no magnetic field is applied ($Ha=0.0$), the difference between two cases without and with Brownian motion in terms of Nu_m is about 6.97% while this difference is decreased by 5.72% for $Ra=10^5$. On the other hand, the effect of Brownian motion is vanished when the Hartmann number is increased especially at high Rayleigh numbers $Ra = 10^5$. For example, at $Ra = 10^5$ and $Ha=60$, for the nanofluid with $\phi=0.04$, Nu_m increases by 3.26%. This occurs due to the magnetic damping effect that suppresses the overall heat transfer in the enclosure and as a result the Brownian motion of nanoparticles is diminished. So, the thermal conductivity of the nanofluids due to the Brownian motion of nanoparticles is neglected compared to the static thermal conductivity based on Maxwell classical correlation.

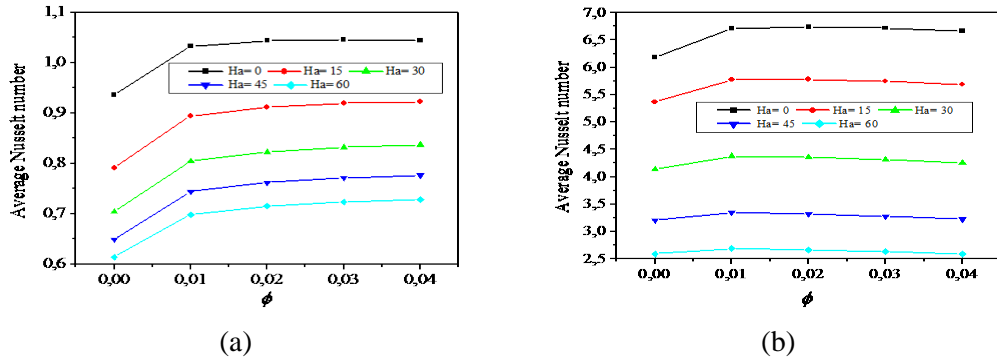


Figure 10: Average Nusselt number on the left wall for different Ra and ϕ , (a) $Ra=10^3$, (b) $Ra=10^5$ at $q = 0$.

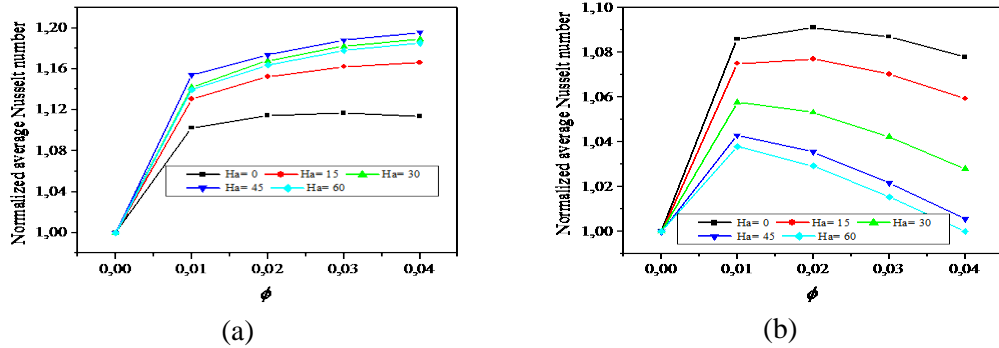


Figure 11: Normalized average Nusselt number on the left wall for different Ra and ϕ , (a) $Ra=10^3$, (b) $Ra=10^5$ at $q = 0$.

Figure 10 presents the influence of the nanoparticles volume fraction (ϕ) and Hartman number (Ha) on the average Nusselt number along the heated surface for different Rayleigh numbers. It demonstrates that the average Nusselt number is raised steadily non-linearly by the augmentation of the nanoparticles at various Rayleigh and Hartmann numbers. It can be seen from these figures that the effect of magnetic field on Nusselt number augments with the enhancement of Rayleigh number. For instance, at $Ra=10^3$ and $\phi= 0.04$, the difference between $Nu_m (Ha=0.0)$ and $Nu_m (Ha=60.0)$ is about 30%, while it is increased by 61% for $Ra=10^5$. This is due to the convection effect which becomes very significant with increasing Rayleigh number and leads to increase the temperature gradient adjacent the hot left sidewall and increases the flow circulation strength. For this reason the Lorentz force due to the application of external magnetic field is neglected compared to the buoyancy force. Figure 11 shows the values of the normalized average Nusselt number at various Rayleigh numbers ($Ra=10^3, 10^5$) for different volume fractions and Hartmann numbers. At $Ra=10^3$, the increase in Hartmann number from $Ha=0$ to 45 acts as an effective parameter to augment heat transfer but the positive impact vanishes from $Ha=45$ to 60.

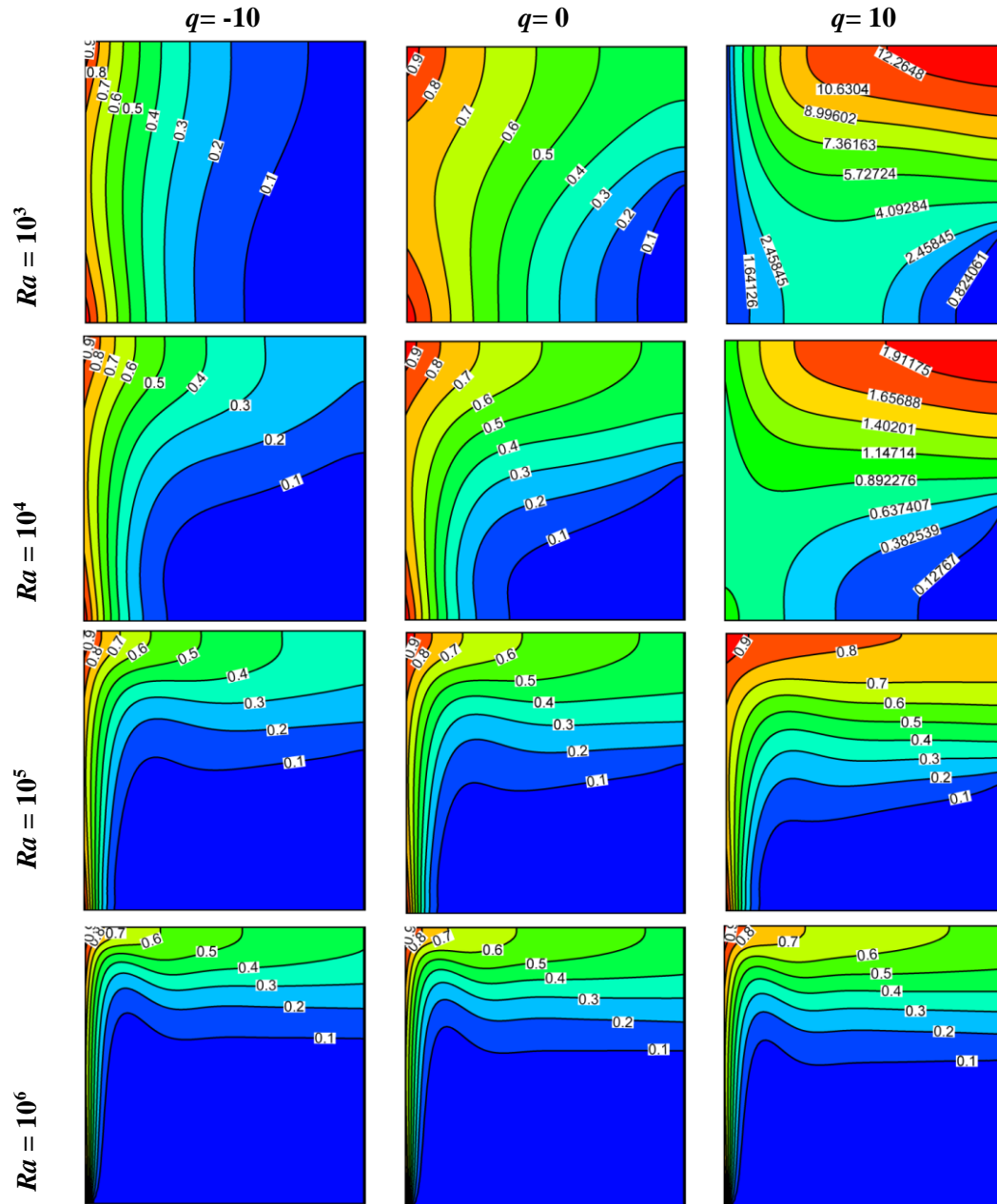


Figure 12: Isotherms for different Ra and q at $Ha=0$ and $\phi=0.04$ (water- Al_2O_3 nanofluid).

Whereas, at $Ra=10^5$, the normalized average Nusselt number demonstrates that heat transfer declines with the enhancement of Hartmann number.

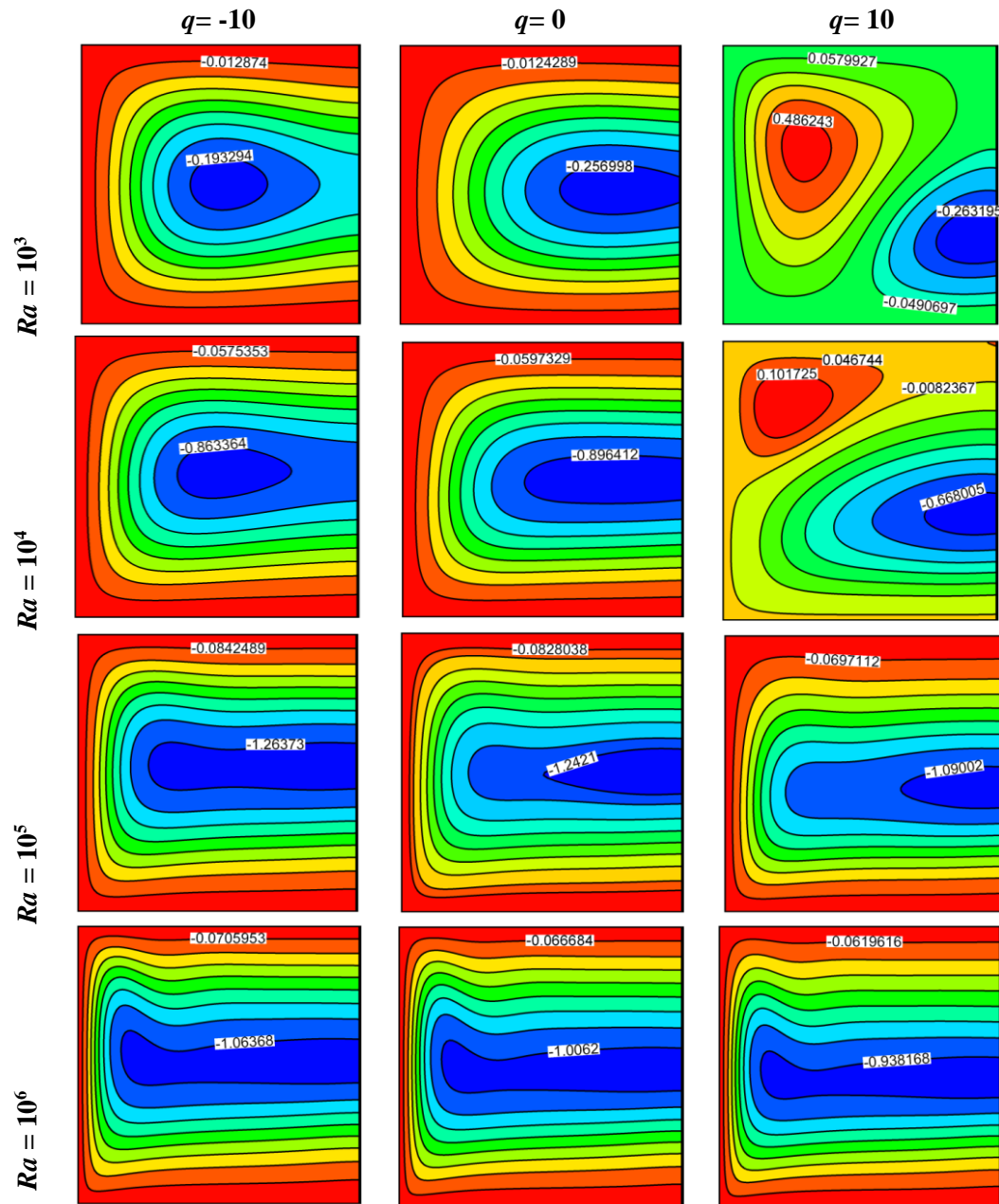


Figure 13: Streamlines for different Ra and q at $Ha=0$ and $\phi=0.04$ (water- Al_2O_3 nanofluid).

Figs. 12-13 illustrates the Rayleigh number effect ($Ra=10^3, 10^4, 10^5$ and 10^6) for different heat generation/absorption and for $Ha=0.0$ on the isotherms and streamlines of nanofluid ($\phi=0.04$). For all heat generation/ absorption coefficients, when Rayleigh number increases; the effect of the convective heat transfer becomes more significant and

boundary layer is formed along the active walls of the cavity. This distribution means that the convective heat mode is predominant. For the case of $q=-10$ (heat absorption), the decrease of the heat absorption coefficient diminishes the nanofluid temperature. Conversely, an opposing effect occurs in the heat generation condition $q=10$, the increase of the heat generation coefficient increases the nanofluid temperature, which decreases the heat transfer at the left wall. Also, as it can be seen from Figure 13, the flow structure changes completely for $Ra=10^3$ and 10^4 . Furthermore, at high Rayleigh numbers ($Ra=10^5$ and 10^6) the maximum value of the stream function declines due to the augmentation of the heat generation/ absorption coefficient. For instance, from $q=-10$ to 10 the values of the maximum stream function decrease by 13.4% and 12.2% for Rayleigh numbers of $Ra=10^5$ and 10^6 respectively.

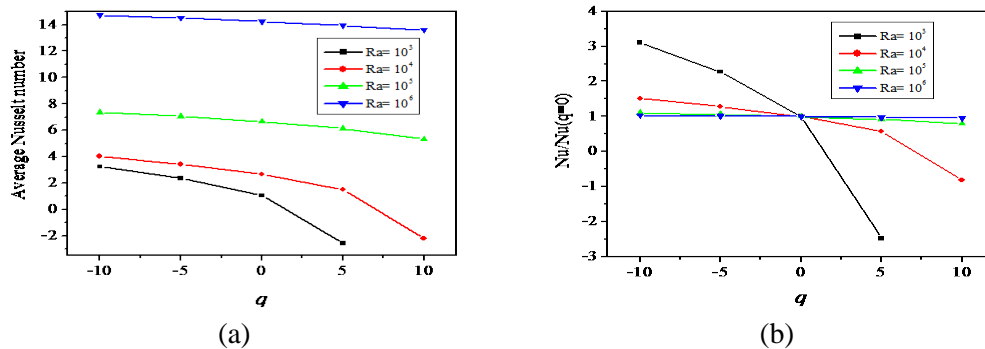


Figure 14: Average and normalized Nusselt number on the left wall for different Ra and q at $Ha=0$ and $\phi=0.04$ (water- Al_2O_3 nanofluid).

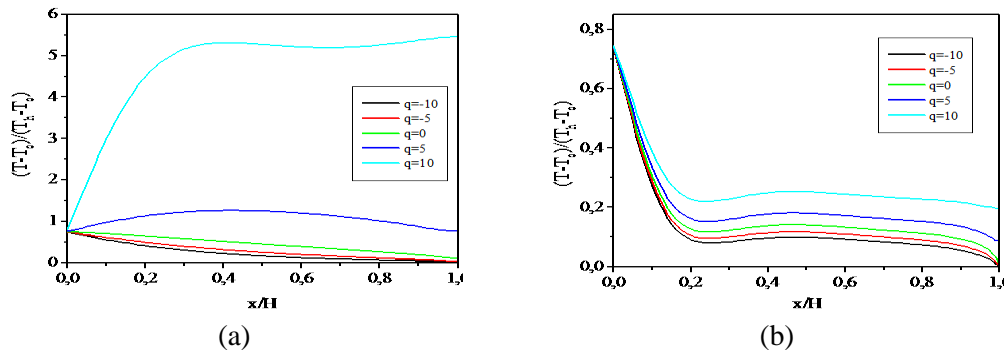


Figure 15: Variation of temperature at $y/H=0.5$ for different q , (a) $Ra=10^3$, (b) $Ra=10^5$ at $Ha=0$ and $\phi=0.04$ (water- Al_2O_3 nanofluid).

Figure 14 illustrates the effect of the heat generation or absorption on the average Nusselt number on the hot wall for different Rayleigh numbers at $\phi=0.04$. Figure 14-a shows that the heat transfer rate on the hot wall decreases with the increase of the heat generation/ absorption coefficient and increases with the rise of Rayleigh numbers. At low Rayleigh numbers ($Ra=10^3-10^4$), when $q > 0$, the nanofluid temperature is higher than the temperature of the hot vertical wall. This leads to negative Nusselt number at the hot wall. On the other hand, the effect of the heat generation or absorption on the average

Nusselt number declines with the enhancement of Rayleigh number. Figure 14-b illustrates the ratio between Nusselt number and Nusselt number without heat generation/absorption. It can be seen that the increase of heat absorption coefficient ($q < 0$), increases the normalized average Nusselt number, especially when the heat absorption coefficient is ($q=-10$). Also, the heat absorption coefficient effect is favored by decreasing the Rayleigh number. Conversely, an opposite effect occurs in the heat absorption condition $q < 0$.

Figure 15a-b show the effect of the heat generation/absorption coefficient respectively for $Ra = 10^3$ and 10^5 on the dimensionless temperature profiles in the middle of the cavity for $Ha=0$ and $\phi = 0.04$. For all heat generation or absorption coefficient, Figure 17a and b show that the dimensionless temperature profiles in the middle of the cavity is greatly affected by changing the Rayleigh number. The changes in amplitudes of temperature decrease with an increase of the heat absorption coefficient ($q < 0$) and increase with an increase of the heat generation coefficient ($q > 0$). For $q = 10$, by increasing Ra from 10^3 to 10^5 , the dimensionless temperature profiles in the middle of the cavity is decreased; its maximum value passes from 5.4 to 0.74.

7 Conclusions

In this study, MHD natural convection heat transfer in an open cavity with non uniform boundary condition in the presence of uniform heat generation/absorption is investigated numerically using the Lattice Boltzmann Method. The effects of nanoparticles volume fraction, Rayleigh numbers, Hartman numbers and heat generation/absorption coefficient on the flow and heat transfer characteristics have been examined.

- Heat transfer is enhanced with the Rayleigh number and decreased as the Hartmann number increases.
- The enhancement in heat transfer is observed at any Rayleigh numbers and nanoparticle volume fraction by considering the role of Brownian motion.
- When Brownian motion is considered, an optimum solid volume fraction can be found, which results in the maximum heat transfer rate.
- The optimum solid volume fraction value depends on the Rayleigh number used.
- The Brownian motion effect is diminished at high Hartmann number ($Ha=60$).
- The heat absorption coefficient effect is favored by decreasing the Rayleigh number. The opposite effect occurs in the case of heat generation coefficient.
- For high Rayleigh number $Ra=10^6$, the effect of heat generation or absorption coefficient is vanished.
- The study of entropy generation, magnetic field orientation, dissipation and Joule effects can be a future work.

References

Aghajani, M.; Farhadi, M.; Sedighi, K. (2009): Effect of the heater location on heat transfer and entropy generation in the cavity using the lattice Boltzmann method. *Heat Trans. Res*, vol. 40, pp. 505-519.

Brinkman, H. C. (1952): The viscosity of concentrated suspensions and solution, *Journal of Chemical and Physics*, vol. 20, pp. 571-581.

Gangawane, K. M.; Bharti, R. P. and Kumar, S. (2016): Effects of heating location and size on natural convection in partially heated open-ended enclosure by using lattice Boltzmann method, *Heat Transfer Engineering*, vol.37, no. 6, pp. 507-522.

Gangawane, K. M.; Bharti, R. P. and Kumar, S. (2015): Lattice Boltzmann analysis of effect of heating location and Rayleigh number on natural convection in partially heated open ended cavity, *Korean Journal of Chemical Engineering*, vol. 32, no. 8, pp. 1498-1514.

Ghasemi, B.; Aminossadati, S. M. (2010): Brownian motion of nanoparticles in a triangular enclosure with natural convection, *International Journal of Thermal Sciences*, vol. 49, pp. 931-940.

Haddad, Z.; Nada, E. A.; Oztop, H. F.; Mataoui, A. (2012): Natural convection in nanofluids: Are the thermophoresis and Brownian motion effects significant in nanofluid heat transfer enhancement, *International Journal of Thermal Sciences*, vol. 57, pp.152-162.

Hussein, A. K.; Ashorynejad, H. R.; Shikholeslami, M.; Sivasankaran, S. (2014) Lattice Boltzmann simulation of natural convection heat transfer in an open enclosure filled with Cuwater nanofluid in a presence of magnetic field, *Nuclear Engineering Design*, vol. 268, pp. 10-17.

Kefayati G. R. (2013): Effect of a magnetic field on natural convection in an open cavity subjugated to water/alumina nanofluid using lattice Boltzmann method. *International Journal of Heat and Mass Transfer*, vol. 40, pp. 67-77.

Kefayati, G. H. R. (2013): Lattice Boltzmann simulation of MHD natural convection in a nanofluid-filled cavity with sinusoidal temperature distribution, *Powder Technology*, vol. 243, pp. 171-183.

Koo, J.; Kleinstreuer, C. (2004): A new thermal conductivity model for nanofluids, *Journal of Nanoparticle Research*, vol. 6, no. 6, pp. 577-588.

Koo, J.; Kleinstreuer, C. (2005): Laminar nanofluid in microheat-sinks. *International Journal of Heat and Mass Transfer*, vol. 48, vol. 13, pp. 2652-2661.

Lage, J. L.; Lim, J. S and Bejan, A. (1992): Natural convection with radiation in a cavity with open top end, *Journal of Heat Transfer*, vol.114, no. 2, pp. 479-486.

Mahmoudi, A.; Mejri, I.; Abbassi, M. A. and Omri, A. (2015): Analysis of MHD natural convection in a nanofluids filled open cavity with non uniform boundary condition in the presence of uniform heat generation/absorption, *Powder Technology*, vol. 269, pp. 275-289.

Mahmoudi, A.; Mejri, I. (2015): MHD natural convection in a nanofluid-filled open enclosure with a sinusoidal boundary condition, *Chemical Engineering Research and Design*, vol. 98, pp. 1-16.

- Mohammad, A. A.; El-Ganaoui, M. and Bennacer, R.** (2009): Lattice Boltzmann simulation of natural convection in an open ended enclosure, *International Journal of Thermal Sciences*, vol. 48, pp. 1870-1875.
- Murshed, S. M. S.; Leong, K.C. and Yang, C.** (2008): Investigations of thermal conductivity and viscosity of nanofluids, *International Journal of Thermal Sciences*, vol. 47, no. 5, pp. 560-568.
- Mliki, B.; Abbassi, M. A. and Omri, A.** (2015): Lattice Boltzmann Simulation of MHD Double Dispersion Natural Convection in a C-shaped Enclosure in the Presence of a Nanofluid, *Fluid Dynamic and Material Processing*, vol.11, no.1, pp. 87-114.
- Sezai, I.; Mohamad, A. A.** (1999): Suppressing free convection from a flat plate with poor conductor ribs, *International Journal of Heat and Mass Transfer*, vol. 42, pp. 2041-2051.
- Sheikholeslami M.; Bandpy M. G. and Ganji D.** (2013): Numerical investigation no fMHD effects on Al₂O₃-water nanofluid flow and heat transfer in asemi-annulus enclosure using LBM, *Energy* vol. 60, pp. 501-510.
- Skok, H.; Ramadhyani, S.; Schoenhals and R. J.** (1991): Natural convection in a side-facing open cavity, *International Journal of Heat and Fluid Flow*, vol. 12, no. 1, pp. 36-45.
- Xuan, Y.; Roetzel, W.** (2000): Conceptions for heat transfer correlation of nanofluids, *International Journal of Heat and Mass Transfer*, vol. 19, pp. 3701-3707.
- Zou, Q.; He, X.** (1997): On pressure and velocity boundary conditions for the lattice Boltzmann BGK model, *Physics of Fluids*, vol. 9, pp. 1591-1598.